Research Paper

Journal of Vascular Research

J Vasc Res 2011;48:429–442
DOI: 10.1159/000324840

Received: October 25, 2010
Accepted after revision: January 27, 2011
Published online: May 31, 2011

Cellular and Molecular Responses of the Basilar Terminus to Hemodynamics during Intracranial Aneurysm Initiation in a Rabbit Model

John Kolega[a, b] Ling Gao[a, c] Max Mandelbaum[a, d] J Mocco[c, g]
Adnan H. Siddiqui[a, c, e] Sabareesh K. Natarajan[a, c, f] Hui Meng[a, c, d]

[a]Toshiba Stroke Research Center, Departments of [b]Pathology and Anatomical Sciences, [c]Neurosurgery, [d]Mechanical and Aerospace Engineering, and [e]Radiology, State University of New York at Buffalo, and [f]Department of Neurosurgery, Millard Fillmore Gates Hospital, Kaleida Health, Buffalo, N.Y., and [g]Department of Neurosurgery, University of Florida, Gainesville, Fla., USA

Key Words
Intracranial aneurysm · Hemodynamic forces · Vascular remodeling · Internal elastic lamina · Matrix metalloproteinase · Apoptosis · Inflammatory cells · Wall shear stress

Abstract
Background/Aims: Hemodynamics constitute a critical factor in the formation of intracranial aneurysms. However, little is known about how intracranial arteries respond to hemodynamic insult and how that response contributes to aneurysm formation. We examined early cellular responses at rabbit basilar termini exposed to hemodynamic insult that initiates aneurysmal remodeling. ***Methods:*** Flow in the basilar artery was increased by bilateral carotid artery ligation. After 2 and 5 days, basilar terminus tissue was examined by immunohistochemistry and quantitative PCR. ***Results:*** Within 2 days of flow increase, internal elastic lamina (IEL) was lost in the periapical region of the bifurcation, which experienced high wall shear stress and positive wall shear stress gradient. Overlying endothelium was still largely present in this region. IEL loss was associated with localized apoptosis and elevated expression of matrix metalloproteinases (MMPs) 2 and 9. A small number of inflammatory cells were sporadically scattered in the bifurcation adventitia and were not concentrated in regions of IEL loss and MMP elevation. Elevated MMP expression colocalized with smooth muscle α-actin in the media. ***Conclusion:*** The initial vascular response to aneurysm-initiating hemodynamic insult includes localized matrix degradation and cell apoptosis. Such destructive remodeling arises from intrinsic mural cells, rather than through inflammatory cell infiltration.

Introduction

An intimate relationship has long been recognized between the formation of intracranial aneurysms and hemodynamics [1, 2]. Intracranial aneurysms are predominantly located at apices of arterial bifurcations or outer curves on or near the circle of Willis [2, 3], where the vessel wall is exposed to a special hemodynamic environment consisting of high frictional force on the wall (wall shear stress, WSS) and significant flow acceleration creating a spatial gradient in WSS (WSS gradient, WSSG)

J.K. and L.G. contributed equally to this work.

KARGER

Fax +41 61 306 12 34
E-Mail karger@karger.ch
www.karger.com

Accessible online at:
www.karger.com/jvr

Dr. John Kolega
Department of Pathology and Anatomical Sciences
State University of New York at Buffalo, 206A Farber Hall
3435 Main Street, Buffalo, NY 14214 (USA)
Tel. +1 716 829 3527, E-Mail kolega@buffalo.edu

[4]. Numerous published cases report patients developing intracranial aneurysms secondary to increases in blood flow associated with incidental occlusions or surgical procedures [5, 6]. Furthermore, in experimental animal models, hypertensive lathrytic rats develop aneurysms, but only after local flow is increased by ligation of the contralateral blood supply [7]. In rats with induced hypertension and collagen cross-linking deficiency [8] or estrogen deficiency [9, 10], flow increase due to carotid ligation is necessary to induce aneurysm formation.

It has been demonstrated that intracranial aneurysms can be induced in rabbits solely by increasing the flow at the basilar terminus, in the absence of any other manipulations or risk factors [11–13]. We have shown that early aneurysmal degradation is strongly localized to regions of the vessel that experience a combination of high WSS and positive WSSG, and that there is a threshold level of WSS and WSSG above which aneurysmal damage almost always occurs [12]. Thus, specific hemodynamic insult appears to be a necessary and sufficient factor for intracranial aneurysm formation. Yet, little is known about how intracranial bifurcations respond at the cellular level to increased flow and how the response could contribute to the initiation of aneurysms in the intracranial vasculature.

Straight vessel segments respond to chronically increased flow by adaptive remodeling, enlarging until shear stress at the vessel wall is returned to baseline levels [14–16]. This adaptive remodeling is a constructive process that includes slight, transient degradation of extracellular matrix to permit expansion of the wall scaffold, synthesis of additional matrix and growth of smooth muscle to enlarge the vessel, and endothelial proliferation to maintain coverage of the enlarged surface [17, 18].

In contrast, development of an aneurysm is a destructive remodeling event, with the wall of the aneurysm exhibiting endothelial damage, loss of internal elastic lamina (IEL), thinning of the media, and inflammatory infiltrates [19, 20]. Because the very early stages of intracranial aneurysm formation have not been observed, it is not clear which of the remodeling events above are direct responses to the initiating insult and which are later sequelae to the initial damage. Moreover, because most aneurysm models include additional manipulations such as lathyrogenic agents and induction of hypertension, it is not known which responses are elicited specifically by hemodynamic insult.

In the present study, we examined the early destructive cellular and molecular responses caused solely by increased flow at an intracranial bifurcation where aneurysmal development has been documented [12, 13, 21]. A sustained increase in flow was induced at the basilar terminus in rabbits by ligation of the carotid arteries, then 2 or 5 days later the basilar bifurcation was examined histologically and biochemically for flow-induced changes indicative of tissue remodeling. Matrix degradation, upregulation of matrix metalloproteinases (MMPs), and increased apoptosis were found to occur very early on, prior to inflammatory infiltration, suggesting that the high-flow hemodynamic environment can elicit destructive remodeling activities from the vessel wall itself.

Methods

Animal Surgery

Adult female New Zealand White rabbits (3–4 kg) were subjected to bilateral common carotid artery (CCA) ligation to increase blood flow to the basilar terminus as reported previously [11, 21]. The animals were euthanized by the intravenous administration of 100 mg/kg of sodium pentobarbital at 2 (n = 3) or 5 days (n = 10; 7 for histology and immunohistochemistry, 3 for quantitative PCR (qPCR) analysis) after ligation. In control rabbits (n = 5; 2 for histology and immunohistochemistry, 3 for qPCR analysis), carotid arteries were exposed but not ligated, and the animals were sacrificed 5 days after the operation. All procedures were in accordance with institutional guidelines for animal experimentation and approved by the local institutional animal care and use committee.

Calculation and Visualization of Hemodynamics

Hemodynamics were determined by computational fluid dynamics as described previously [12, 22, 23]. Briefly, high-resolution three-dimensional rotational digital subtraction cerebral angiography was performed immediately after CCA ligation and just before sacrifice using a Toshiba Infinix VS-i system to obtain vessel geometries. Blood velocity was measured in the basilar artery in the conscious rabbits before ligation (baseline; day 0) and on postligation day 1 (after convalescence from the surgery) using transcranial Doppler sonography (Spencer Technology). Computational fluid dynamics analysis was performed on the three-dimensional image of the basilar bifurcation to obtain baseline and postligation flow fields, using the pre- and postligation velocity measurements as the inlet boundary conditions, respectively.

RNA Isolation and Quantitative PCR

Five days after bilateral ligation (n = 3) or sham surgery (n = 3), immediately after sacrifice, the basilar bifurcation of rabbits were excised in RNAlater reagent (Qiagen). Approximately 1 mm of the periapical region was dissected, and the total RNA was extracted from the tissues using the RNAeasy MicroKit (Qiagen). The cDNA was synthesized from approximately 100–200 ng of total RNA using a QuantiTect Reverse Transcriptase kit (Qiagen), according to the manufacture's instruction. qPCR was performed with primers specific to rabbit MMP-2 or MMP-9 using 1/20 of synthesized cDNA with iQ SYBR green supermix (Bio-Rad) and MyiQ single-color real-time PCR detection system (Bio-Rad).

18S rRNA was used as a reference gene. The primers sets used were: forward 5′-TGTGTCTTCCCCTTCGTCTT-3′, reverse 5′-CCCCACTTCTTGTCGCTGT-3′ for MMP-9; forward 5′-CATGTCTACTATTGGCGGGAAC-3′, reverse 5′-TAACCTTGGTCAGGGCAGAA-3′ for MMP2; forward 5′- GGACAGGATTGACAGATTGATAG-3′, reverse 5′-CGGACATCTAAGGGCATCAC-3′ for 18SrRNA. The conditions for qPCR reaction were an initial denaturing at 95°C for 3 min, followed by 40 cycles of 95°C for 10 s and 60°C for 30 s. A melting-curve analysis was performed to confirm the absence of primer dimers and other nonspecific PCR products. The amount of mRNA was expressed as the ratio to 18S rRNA mRNA.

Tissue Preparation for Immunohistochemistry

Immediately after sacrifice, the vertebral arteries were perfused with phosphate-buffered saline and pressure fixed in situ at 150 mm Hg with 10% buffered neutral formalin for 30 min. The vessels were fixed at this slightly elevated pressure to prevent vasospasm and to compensate for the shrinkage that is associated with the fixation process. The brain was removed and fixed in 10% buffered neutral formalin for 24 h. The basilar bifurcation was excised, embedded in paraffin and sectioned longitudinally. Adjacent, 4-μm-thick sections from the median plane of the bifurcation were used for Van Gieson staining for signs of destructive aneurysmal remodeling, and immunohistochemistry staining for molecular and cellular changes.

For immunohistochemical analysis, sections were deparaffinized, rehydrated and incubated with 0.3% H_2O_2 for 5 min to inactivate endogenous peroxidase. Antigen was unmasked by boiling sections in 10 mM citric buffer (pH 6.0). Sections were then stained with mouse monoclonal antibodies: anti-MMP-2 (Chemicon), anti-MMP-9 (Chemicon), PECAM-1 (a gift from Dr. Peter Newman), RAM11 recognizing macrophages (Dako), MCA805G recognizing neutrophils and T lymphocytes (AbD Serotec), and visualized with EnVision+ System-HRP (DAB) kit (Dako).

Cell apoptosis in the basilar bifurcation was examined by a TUNEL assay to detect DNA fragmentation in apoptotic cells using the ApopTaq Plus Peroxidase in situ Apoptosis Detection Kit (Chemicon).

For double immunofluorescence staining, smooth muscle cytoplasm was stained using a monoclonal antibody to α-actin (Abcam) labeled with Zenon IgG_{2a} Alexafluor 488 probes (Invitrogen) and either MMP-2 or MMP-9 antibody labeled with Zenon IgG_1 Alexafluor 568 probes (Invitrogen). Fluorescence was imaged with a Zeiss Axio Imager Z1 microscope with excitation/emission wavelengths of 495/519 and 578/603 for the 488 and the 568 probes, respectively.

Quantitation of Immunohistochemistry

Digital color images of stained slides were captured using a 40× objective of a Zeiss Axioskop microscope equipped with a Hitachi KP-D50U color digital camera and FlashPoint three-dimensional FPG 1.5 software (Integral Technology Inc). Quantitation of immunohistochemistry was performed using ImageJ software (NIH). The yellow channel was extracted from the CMYK color scheme in order to obtain the best contrast and intensity scale of the image, and to eliminate background as much as possible [24]. The immunohistochemistry was quantified in four regions of the basilar bifurcation: the periapical region with high WSS and high, positive WSSG, the left posterior cerebral artery, the right posterior cerebral artery and the basilar artery. Due to slight variation in background between slides, the intensity threshold used to define positive staining for each stained section was determined by the following method: the intensity histogram for the entire basilar artery was obtained and the mean and standard deviation of the intensities calculated. The threshold value for positive staining was taken as the mean basilar artery intensity plus 2 standard deviations.

Statistical Analysis

All values are expressed as means ± standard error of mean. Statistical analyses were performed using Systat 11 software for Mann-Whitney U tests and GraphPad Instat 3.0 software for all others. Paired and unpaired t tests were used to test for statistical significance of MMP-2 and MMP-9 protein expression levels, and Mann-Whitney U tests were used to compare MMP-2 and MMP-9 mRNA levels as specified in the Results section. One-way ANOVA with Bonferroni post hoc correction was used to test for statistical significance of apoptotic cells and inflammatory cells across multiple regions of interest. For all statistical tests, differences were considered significant at $p < 0.05$.

Results

IEL Was Rapidly Damaged during Hemodynamic Insult

Histological examination of the basilar terminus after carotid ligation revealed a number of structural changes as early as 2 days after CCA ligation (table 1). The most conspicuous morphological change was prominent and consistent loss of the IEL in the periapical region. In all rabbits subjected to carotid ligation (both 2 and 5 days), IEL was degraded in segments of the basilar terminus around the apex of the bifurcation (fig. 1c, e), whereas none of the rabbits that had sham surgery exhibited any IEL loss (fig. 1a). The average length of IEL loss at 2 and 5 days was 261 ± 110 and 358 ± 100 μm, respectively. Loss of IEL was consistently localized either in segments flanking the apex or continuously extending from one side to the other including the apex (fig. 1c, e), which corresponds to the region that experiences high WSS and high, positive WSSG as illustrated in figure 1g.

Apoptosis and Changes in Media Structure Also Occurred in Regions with IEL Loss

In addition to IEL degradation, one of three 2-day ligated rabbits (33%) and six of seven 5-day ligated rabbits (86%) exhibited localized thinning of the media and outward bulging of the lumen as previously reported [12, 13] (fig. 1e), indicating progression of aneurysmal changes of the 5-day rabbits compared to the 2-day rabbits. Because

Table 1. Frequency of destructive events in the periapical region of the basilar terminus

	Sham (n = 3)	2 days after ligation (n = 3)	5 days after ligation (n = 7)
Number of basilar termini with IEL loss	0	3	7
Number of basilar termini with media thinning and vessel bulging	0	1	6
Number of basilar termini with apoptotic cells in			
any layer of the vessel wall	0	3	7
the intima	0	0	5
the media	0	2	2
the adventitia	0	3	3
Number of basilar termini with endothelial loss or discontinuity	0	1	1

Each evaluation was confirmed by the assessments of 2 blinded observers.

the structure of the wall is predominantly due to the smooth muscle layers, we examined whether there is loss of cells through apoptosis in the vessel wall. TUNEL assays did not detect any apoptotic cells in the periapical area of sham-operated control rabbits (table 1; fig. 2a), but revealed apoptotic cells in the vessel wall around the apex in all animals 2 and 5 days after ligation (table 1; fig. 2b, c). The apoptotic cells were found in all 3 layers of the wall (intima, media and adventitia) and were tightly clustered around the bifurcation apex, that is, within the area of high WSS, high positive WSSG and where destructive remodeling was indicated by IEL disruption. This localization of apoptosis was confirmed by quantifying the distribution of apoptotic cells in the basilar bifurcations and specifically comparing the periapical region with the inlet vessel (basilar artery) and outlet vessels (posterior cerebral arteries) as shown in figure 2d. At 2 days, significantly more apoptotic cells were found in the periapical area than in the right or left posterior cerebral artery or the basilar artery (1.37 ± 0.20 vs. 0 ± 0, 0.13 ± 0.13 and 0 ± 0 cells/mm, respectively; $p < 0.01$ in all 3 comparisons), and the same was true at 5 days (1.29 ± 0.43 cells/mm in the peri-apical region vs. 0.14 ± 0.06, 0.06 ± 0.04 and 0.11 ± 0.06 cells/mm for the right and left posterior cerebral arteries and the basilar artery, respectively; $p < 0.01$).

MMP-2 and MMP-9 Were Elevated in the IEL Destruction Region

The observed IEL loss, media changes and apoptosis were accompanied by increases in the matrix proteases, MMP-2 and MMP-9. qPCR analysis of tissue dissected from the basilar terminus showed that both MMP-2 and MMP-9 mRNA were significantly increased in the periapical region of 5-day ligated rabbits compared with controls (fig. 3) [mRNA level relative to 18S rRNA: $(2.06 \pm 0.19) \times 10^{-4}$ in ligated rabbits vs. $(0.91 \pm 0.15) \times 10^{-4}$ in controls for MMP-2, and $(0.14 \pm 0.02) \times 10^{-4}$ vs. $(0.04 \pm 0.02) \times 10^{-4}$ for MMP-9, $p < 0.01$].

Because the periapical region (where IEL degradation occurred) was too small to provide sufficient tissue for biochemical quantitation of protein levels, we examined MMP-2 and MMP-9 protein expression by immunohistochemistry, which also permitted us to examine the spatial distribution of these proteins relative to the hemodynamic microenvironment. In controls, MMP-2 staining was weak and at a similar level in all cell layers of the periapical region (fig. 4a, b). In both 2-day and 5-day ligated rabbits, the MMP-2 expression was increased throughout all of the basilar bifurcation and appeared greatest in the periapical areas with IEL destruction (fig. 4c–f).

To verify that MMP-2 expression was most elevated in the regions subjected to high WSS and positive WSSG, the immunostaining was quantified in four regions of the basilar bifurcation: (1) the periapical area, which was exposed to high WSS and positive WSSG and suffered IEL loss, (2) the left and (3) the right downstream branches (posterior communicating arteries), where flow was decelerating and thus the wall experienced high WSS and negative WSSG, and (4) the inlet vessel (basilar artery), which experienced elevated flow and WSS, but no spatial gradient. The percentage of area that was positively stained in each region is shown in figure 4d. At 2 days, elevated staining was present in 18.5 ± 3.9% of the periapical region versus 6.1 ± 1.7 and 7.5 ± 2.4% for the right and left posterior cerebral arteries, respectively, as well as 4.5 ± 1.6% in the basilar artery. At 5 days, the periapical region was 7.4 ± 1.4% positive versus 3.3 ± 0.7 and 2.7

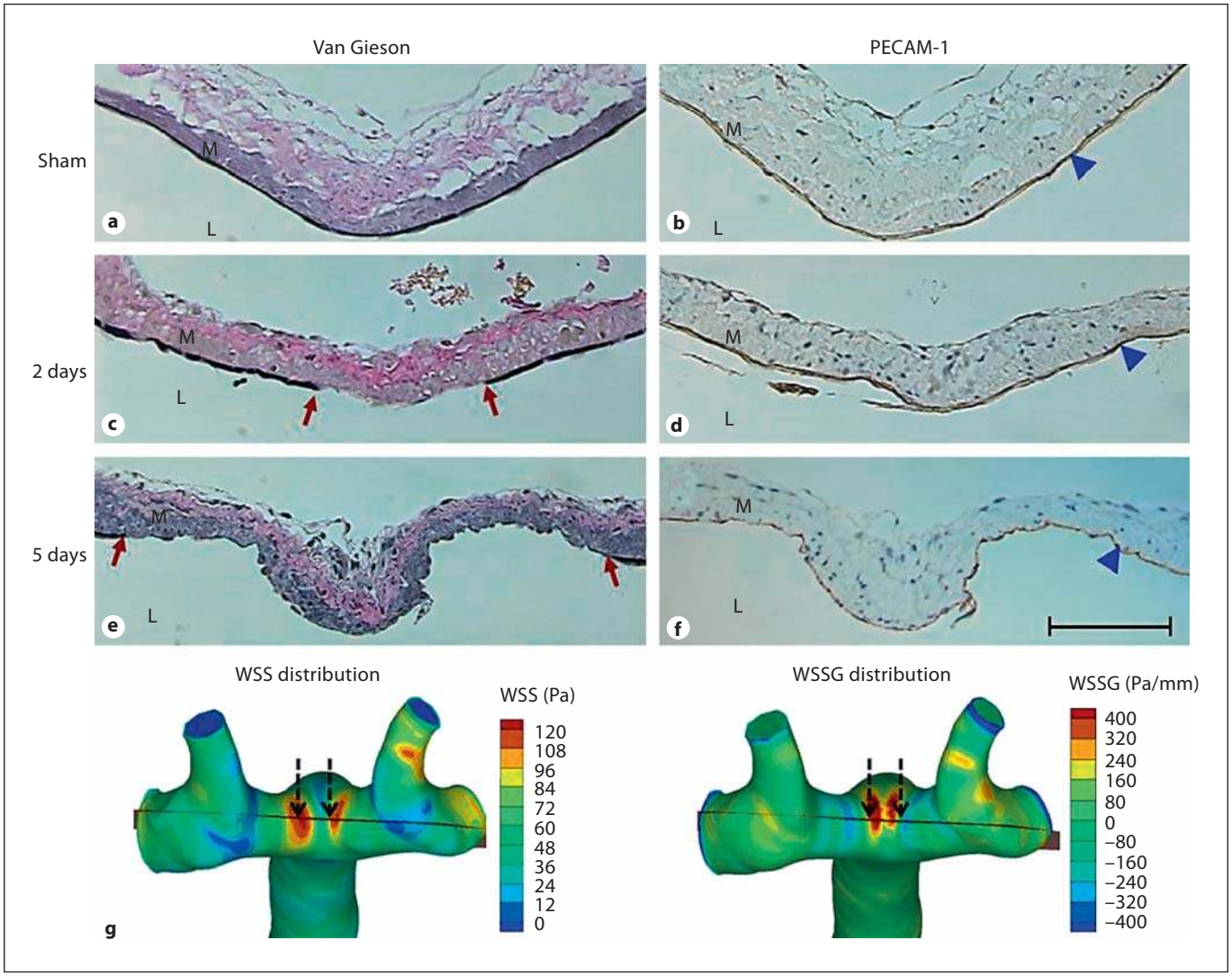

Fig. 1. Rabbit basilar terminus histology (**a–f**) and hemodynamic stress distributions (**g**). Van Gieson staining shows an intact IEL in the sham control group (**a**) and loss of IEL in the periapical region 2 days after carotid ligation (**c**) and 5 days after ligation (**e**); IEL is absent between red arrows. **b**, **d**, **f** Adjacent sections to those shown in **a**, **c** and **e** were stained for PECAM-1 (brown) and counterstained with hematoxylin (blue). A continuous, PECAM-1-positive endothelium (indicated by blue arrow head) is seen in all 3 cases. At 5 days after ligation, medial thinning (**e**) and bulging (**e**, **f**) were also evident. L = Lumen; M = media. Scale bar = 100 μm. **g**. Three-dimensional representation of the WSS and WSSG distribution that was sectioned for **e** and **f**. Highest WSS values are very strongly localized to small segments on either side of the apex, with the highest WSSG values occurring even closer to the apex – as flow accelerates away from the apex to the WSS maxima. The brown planes through the three-dimensional renderings show the cutting plane for the sections in **e** and **f**, and the dashed arrows indicate the lateral edges of those sections. Note that this segment of the wall experiences both high WSS and high positive WSSG, and that this combination of hemodynamics is unique to this location.

± 1.7% in the right and left posterior cerebral arteries, respectively, as well as 1.6 ± 0.2% in the basilar. Paired t tests indicated that MMP-2 expression was elevated in a greater proportion of the periapical area than in each other segment at both 2 and 5 days ($p < 0.05$). Furthermore, MMP-2 was more broadly elevated in the periapical area at 2 days than at 5 days (18.5 ± 3.9 vs. 7.4 ± 1.4%, $p < 0.05$). Thus, a localized increase in MMP-2 expression occurred within 2 days of the onset of hemodynamic insult, but was already subsiding by 5 days.

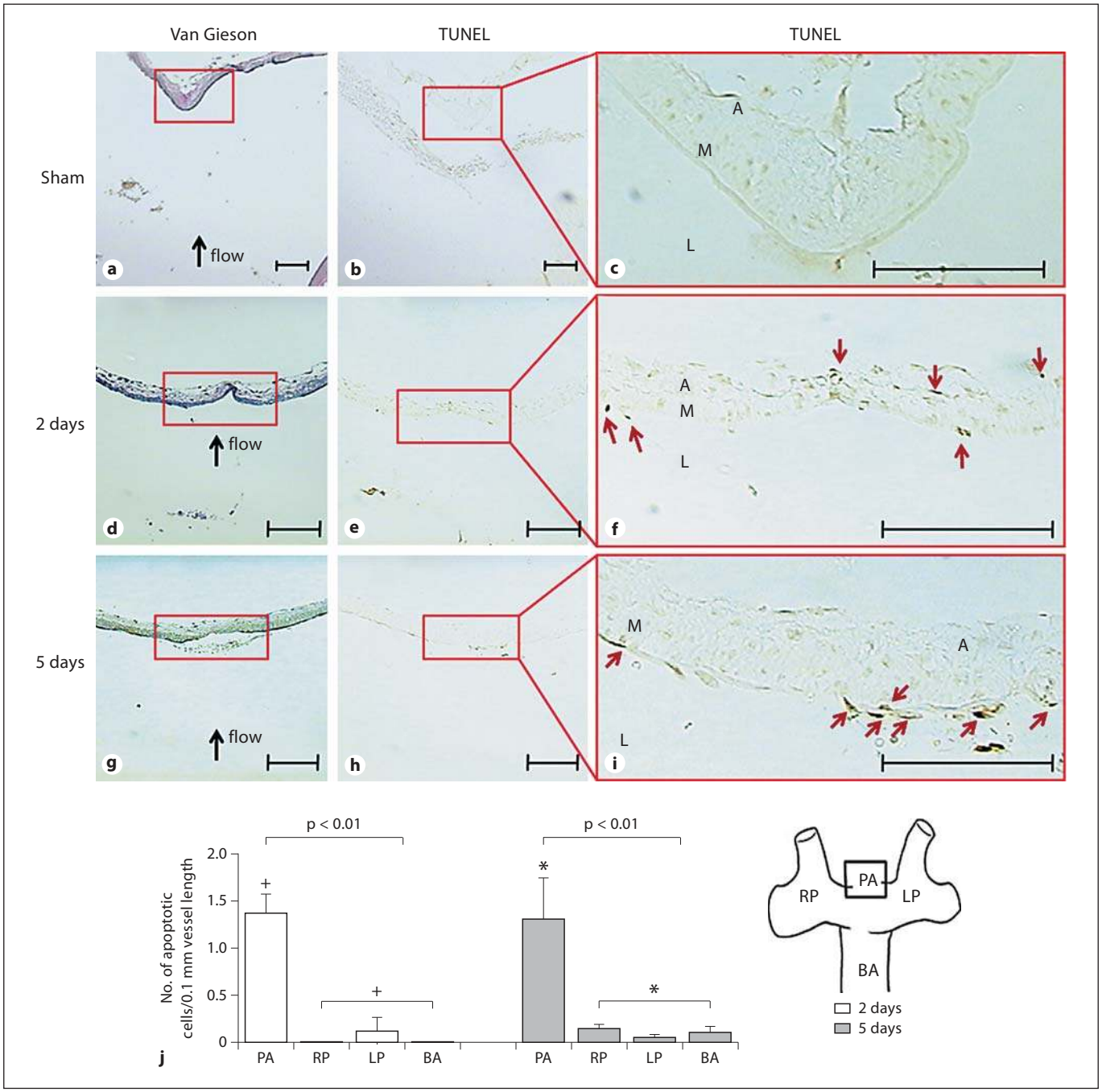

Fig. 2. TUNEL staining of the basilar terminus. Apoptotic cells clustered in regions with IEL disruption at both 2 and 5 days after bilateral carotid ligation. **a**, **d**, **g** IEL destruction indicated by Van Gieson staining. **b**, **c**, **e**, **f**, **h**, **i** Apoptosis was detected by TUNEL staining, and is marked by red arrows. **a–c** Sham control. **d–f** Two days after ligation. **g–i** Five days after ligation. M = Media; L = lumen; A = adventitia. Scale bars = 100 μm. **j** Tissue sections were divided into 4 regions as indicated in the diagram, and TUNEL-positive cells were counted over a vessel length of approximately 500 μm in each region. The 4 regions are the periapical area (PA), right posterior cerebral artery (RP), left posterior cerebral artery (LP) and basilar artery (BA). One-way ANOVA analysis with Bonferroni post hoc correction indicated that the number of apoptotic cells in the periapical area was significantly higher than other areas at both 2 and 5 days. $^{+}$ $p < 0.01$, periapical area compared with other segments at 2 days. * $p < 0.01$, periapical area compared with other segments at 5 days.

Increased and localized protein expression was also observed for MMP-9. Immunohistochemistry indicated that control rabbits had very weak MMP-9 staining and expressed MMP-9 at a similar level in all cell layers of the periapical area (fig. 5a, b). In both 2- and 5-day ligated rabbits, MMP-9 was significantly elevated and localized in the region of IEL disruption (fig. 5c–f). MMP-9 was observed in both the adventitia and the media, with stronger staining associated with the cellular portions than with the interstitial matrix (fig. 5f). Quantitation of MMP-9 immunohistochemistry confirmed that elevated expression occurred preferentially in the periapical region of both 2- and 5-day ligated rabbits compared to the inlet and outlet arteries (fig. 5d). At 2 days, the periapical region was 18.0 ± 3.1% positive versus 3.9 ± 1.4 and 7.4 ± 3.9% in the right and left posterior cerebral arteries, respectively, as well as 4.5 ± 1.9% in the basilar artery. At 5 days, the periapical tissue was 27.4 ± 3.4% positive versus 10.3 ± 2.3 and 12.3 ± 3.9% in the right and left posterior cerebral arteries, respectively, as well as 12.9 ± 2.6% in the basilar. Like MMP-2, MMP-9 was significantly higher in the periapical region in all instances ($p < 0.005$, paired Students t tests). However, in contrast to MMP-2, MMP-9 was more broadly elevated in the periapical area at 5 days than at 2 days (27.4 ± 3.4 vs. 18.0 ± 3.1%, $p < 0.05$). Thus, the localized elevation of MMP-9 expression continued to increase to at least 5 days after ligation.

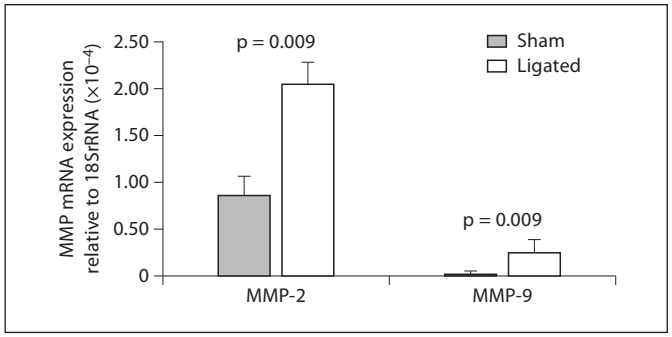

Fig. 3. qPCR analysis showing increased MMP-2 and MMP-9 mRNA expression at the periapical area of 5-day ligated rabbits compared with sham control. The expression level of each sample is expressed as the ratio to 18SrRNA. The p value for MMP-2 or MMP-9 shown on the top of each graph is from unpaired t test comparing ligated to sham.

IEL Damage Frequently Occurred without Loss of the Overlying Endothelium

Because the increased shear stresses created by increased flow are initially felt only by the endothelium, we examined the integrity of the endothelium using PECAM-1 as an immunohistochemical marker. Somewhat surprisingly, we found an intact endothelium at the basilar terminus in most ligated animals, even when the underlying IEL was damaged (table 1). One 2-day rabbit had no PECAM-1 staining over the IEL-damage region, and one 5-day rabbit had small isolated discontinuities in the PECAM-1-positive layer, but all 6 remaining ligated rabbits displayed uniform PECAM-1 staining across the periapical surface, including regions where the IEL was clearly degraded (fig. 1d, f).

IEL Damage and MMP Expression Did Not Correspond to Inflammatory Cell Distributions

Because MMPs were locally elevated in the periapical region of both 2- and 5-day ligated rabbits, we looked for neutrophils, T lymphocytes and macrophages as potential sources. All three cell types were rare in the periapical region of both control and ligated animals (table 2). One of two control rabbits, one of three 2-day rabbits, and four of seven 5-day rabbits had no detectable neutrophils or T lymphocytes at all. In animals that had neutrophils or T lymphocytes, only a single cell or a few, very sparsely distributed cells were detected. No macrophages were found in the basilar terminus of control animals, but a few macrophages were found in the periapical region of some ligated rabbits (three of three 2-day rabbits and two of seven 5-day rabbits). However, whenever neutrophils, T lymphocytes or macrophages were present, they were scattered around the whole bifurcation (table 2); ANOVA showed no preferential localization to the periapical region where MMP expression and IEL loss were observed or any other region ($p > 0.05$). Furthermore, neutrophils, T lymphocytes or macrophages were found exclusively in the adventitia and never near the luminal side of the vessel wall where the IEL lies. Figure 6 shows a bifurcation with clear IEL loss and no inflammatory cells as well as a segment of the basal artery with intact IEL and several adventitial macrophages and neutrophils, illustrating the lack of correlation between the presence of adventitial inflammatory cells and loss of the IEL.

MMP-2 and MMP-9 Were Expressed in Smooth Muscle Cells

Because MMP-2 and MMP-9 were distributed predominantly in the media, we examined whether they might be produced at least in part by smooth muscle cells. Using α-actin as a marker for smooth muscle cytoplasm,

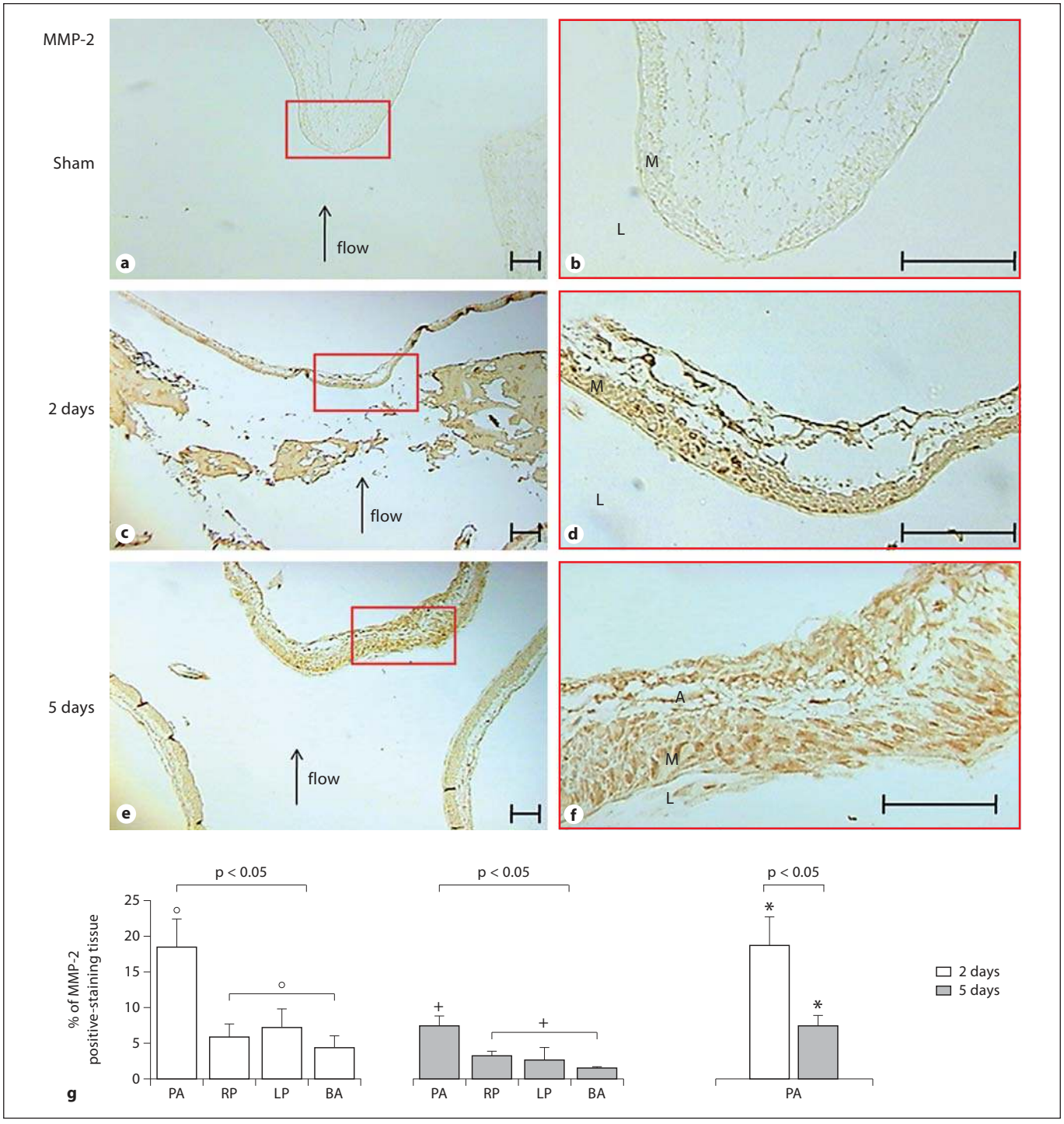

Fig. 4. Immunohistochemistry showing increased MMP-2 in the periapical region of ligated rabbits. **a–f** MMP-2 immunostaining. **a**, **b** Sham control. **c**, **d** Two days after ligation. **e**, **f** Five days after ligation. M = Media; L = lumen; A = adventitia. Scale bars = 100 μm. **g** Quantitation of MMP-2 immunohistochemistry. Paired t tests indicated that the percentage of MMP-2 positive-staining tissues at the periapical area is significantly higher than other segments at both 2 days and 5 days. ° $p < 0.05$, periapical area compared with other segments at 2 days; $^{+}$ $p < 0.05$, periapical area compared with other segments at 5 days. Unpaired t test indicated that the percentage of MMP-2 positive-staining tissue at the periapical area at 2 days is significantly higher than at 5 days. * $p < 0.05$, periapical area at 2 days compared with periapical area at 5 days. PA = Periapical area; LP = left PCA; RP = right PCA; BA = basilar artery.

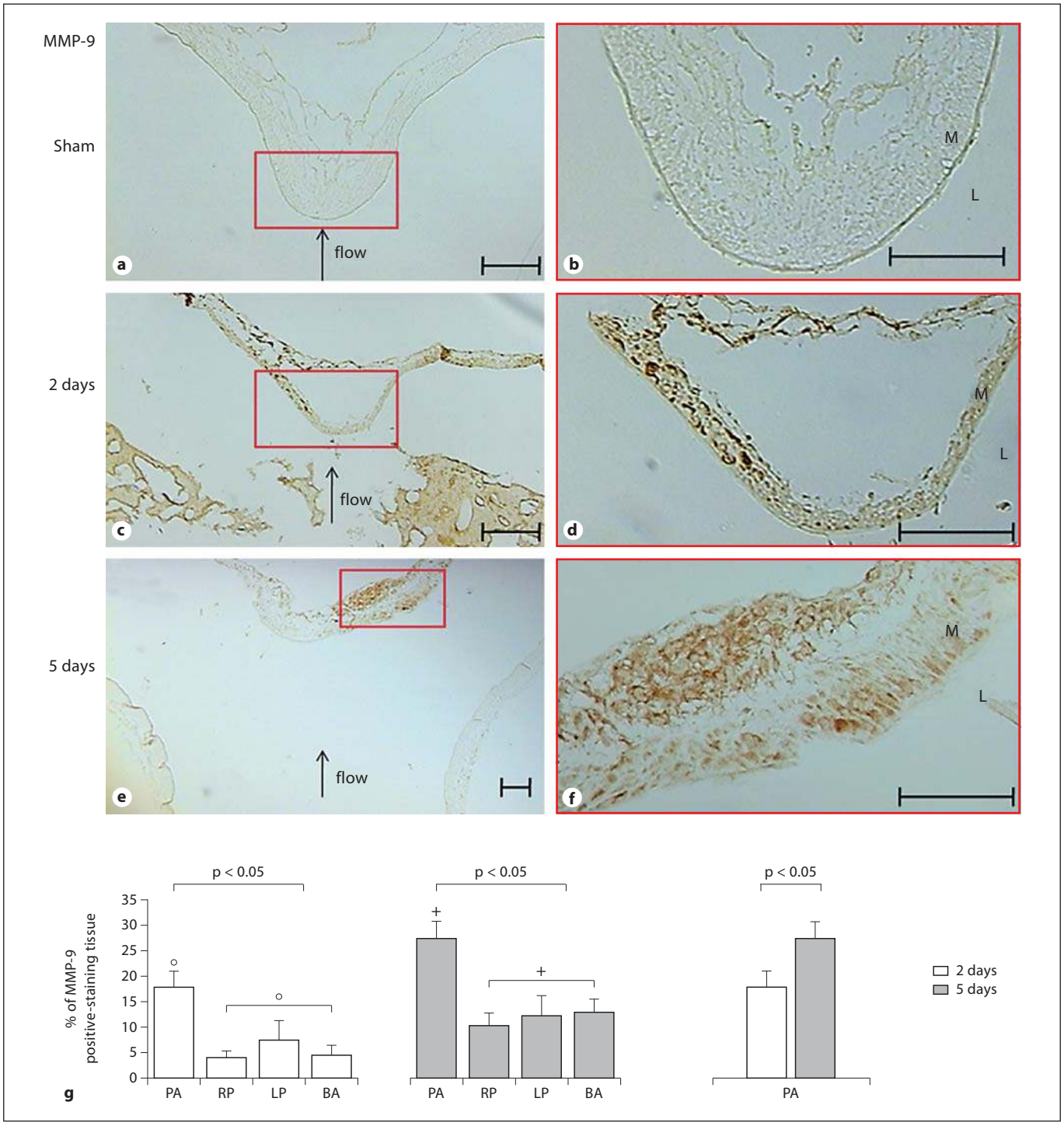

Fig. 5. Immunohistochemistry showing increased MMP-9 in the periapical region of ligated rabbits. **a–f** MMP-9 immunostaining. **a**, **b** Sham control. **c**, **d** Two days after ligation. **e**, **f** Five days after ligation. M = Media; L = lumen; A = adventitia. Scale bars = 100 μm. **g** Quantitation of MMP-9 immunohistochemistry. Paired t tests indicated that the percentage of MMP-9 positive-staining tissues at the periapical area is significantly higher than other segments at both 2 days and 5 days. ° $p < 0.05$, periapical area compared with other segments at 2 days; $^{+}$ $p < 0.05$, periapical area compared with other segments at 5 days. Unpaired t test indicated that the percentage of MMP-9 positive-staining tissue at the periapical area at 5 days is significantly higher than at 2 days. * $p < 0.05$, periapical area at 2 days compared with periapical area at 5 days. PA = Periapical region; LP = left PCA; RP = right PCA; BA = basilar artery.

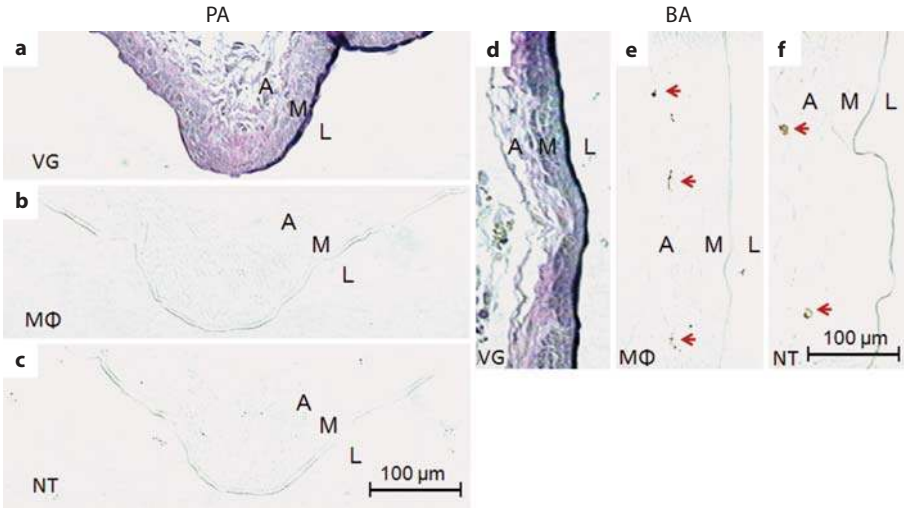

Fig. 6. Lack of correlation between inflammatory cells and IEL damage. The periapical area and the basilar artery of rabbits 5 days after carotid ligation are shown. **a**, **d** Van Gieson staining to show IEL. **a–c** IEL is almost completely lost from the left side of the apex, but immunohistochemistry reveals no macrophages (**b**) or neutrophils and T lymphocytes (**c**) anywhere in the tissue. **d–f** IEL is still completely intact in the basilar artery. Both macrophages (**e**, arrows) and neutrophils and T lymphocytes (**f**, arrows) are observed, and only in the adventitia. M = Media; L = lumen; A = adventitia; VG = Van Gieson; MΦ = macrophages; NT = neutrophils and T lymphocytes; PA = periapical region; BA = basilar artery.

Table 2. Number of inflammatory cells (per 1 mm of vessel length) in and around the basilar terminus in sham and ligated rabbits

Cell locations	Macrophages			Neutrophils and T lymphocytes		
	intima	media	adventitia	intima	media	adventitia
Periapical region of basilar terminus						
Sham surgery	0	0	0	0	0	1.2 ± 1.2
2 days after carotid ligation	0	0	4.8 ± 1.9	0	0	3.4 ± 2.2
5 days after carotid ligation	0	0	1.0 ± 0.7	0	0	1.9 ± 1.3
Right posterior cerebral artery						
Sham	0	0	0.4 ± 0.4	0	0	0.7 ± 0.2
2 days	0	0	1.4 ± 0.2	0	0	3.9 ± 3.6
5 days	0	0	0.9 ± 0.5	0	0	1.9 ± 0.8
Left posterior cerebral artery						
Sham	0	0	0.1 ± 0.1	0	0	1.1 ± 0.5
2 days	0	0	1.1 ± 0.2	0	0	1.1 ± 0.4
5 days	0	0	0.9 ± 0.3	0	0	2.1 ± 0.7
Basilar artery						
Sham	0	0	0.4 ± 0.4	0	0	0.9 ± 0.04
2 days	0	0	1.7 ± 0.6	0	0	6.7 ± 4.9
5 days	0	0	0.4 ± 0.2	0	0	1.3 ± 0.4

double immunofluorescence staining revealed extensive regions of overlap between smooth muscle cells and both MMP-2 and MMP-9 (fig. 7). In particular, smooth muscle cells filled those regions of the media flanking the apex where local upregulation of MMPs was most prominent (asterisk in fig. 7). MMPs were distributed not only in the extracellular space surrounding the smooth muscle cells, but also co-localized with α-actin in the smooth muscle cytoplasm.

Discussion

We have previously shown that bilateral CCA ligation results in well-developed aneurysmal morphology at the basilar terminus after 12 and 27 weeks elapsed, including outward bulging and thinning of the vessel wall [13, 21]. The present experiments show that similar alterations in the hemodynamics cause rapid, localized destructive changes in the vascular wall that are visible as early as 2 days after flow is increased. Because no other manipula-

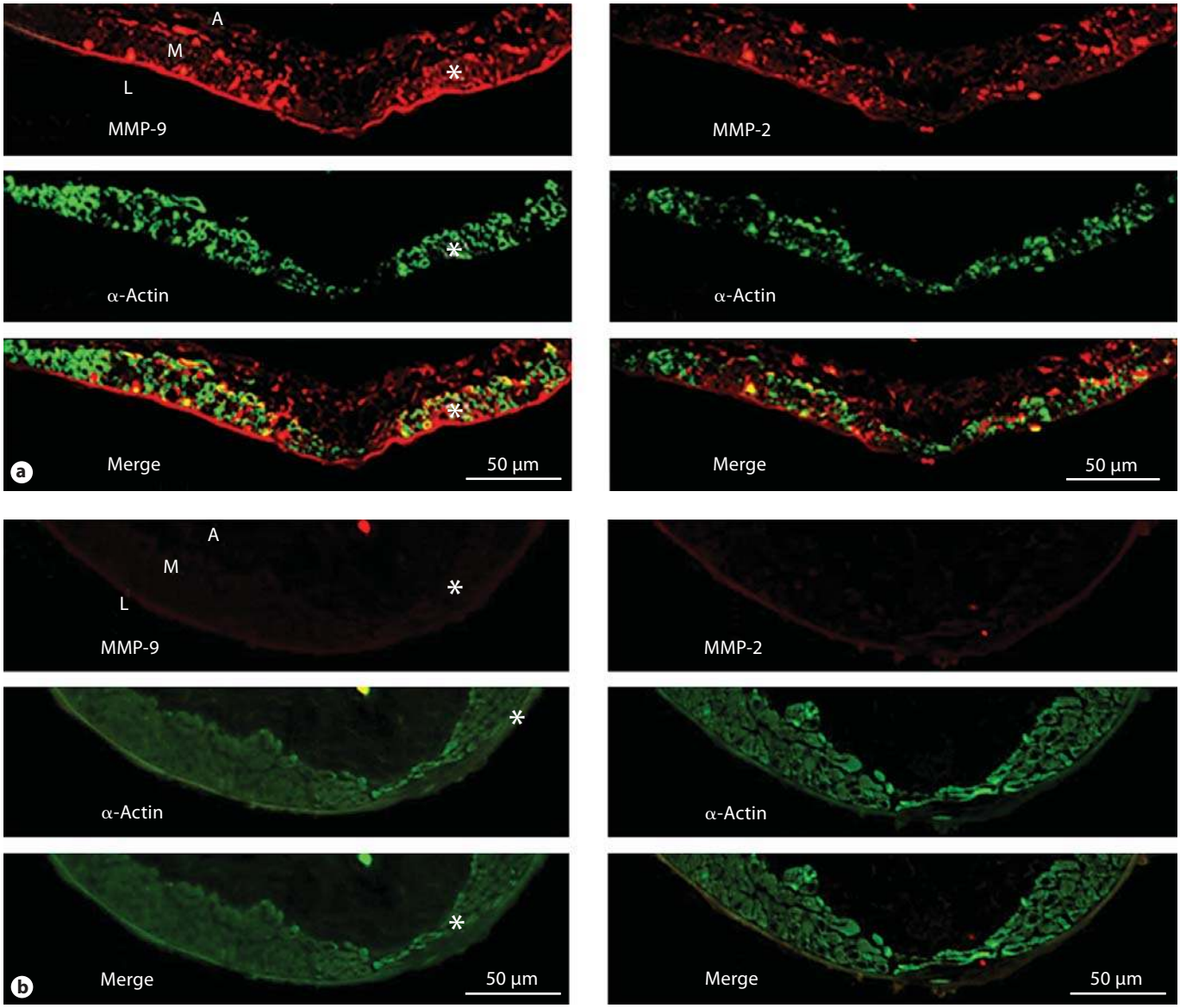

Fig. 7. Double immunofluorescence of MMPs and smooth muscle cells. **a** The periapical area of rabbits 2 days after carotid ligation were stained for α-actin (green) and either MMP-9 or MMP-2 (red). Note the preponderance of MMP-9 in the media flanking the apex and the strong co-localization with α-actin in this region (asterisk). **b** The basilar terminus of a sham-operated rabbit, stained as in **a**, shows very little staining for MMP-2 or MMP-9. Note that α-actin is much more uniformly expressed in the media of the sham-operated tissue than in the ligated bifurcation.

tions were performed, these changes can be attributed to a direct response of the vessel wall to the altered flow environment and thus provide important insight into how hemodynamic insult could contribute to aneurysm initiation.

A prominent feature of the flow-induced response at the basilar terminus is increased matrix degradation, as indicated by IEL loss and upregulation of MMPs. MMP expression and matrix degradation have been widely observed in aneurysms at much later stages, and such activity is likely to thin and weaken the vessel wall, particularly as the IEL is the primary load-bearing element in cerebral arteries [25].

MMP expression has been associated with inflammatory infiltrates in intracranial aneurysms in hypertensive rats [26]. Additionally, elevated MMP-2 and MMP-9 [27,

28] as well as inflammatory cells [19, 20] are found in human intracranial aneurysms. Consequently, extracellular matrix degradation in aneurysms is widely attributed to MMPs released by infiltrated macrophages [26]. However, in the present study, the sporadic occurrence of macrophages, neutrophils, and T lymphocytes was not associated with IEL degradation and MMP accumulation: they were found in the adventitia and not in the intima, they displayed no preferential distribution in damaged vessel segments, and they did not colocalize with elevated MMP-2 and MMP-9. These results contrast with the behavior previously reported in a rodent aneurysm model, where macrophages infiltrated the intima and media in aneurysms 1 month after induction, and also infiltrated the adventitia in advanced aneurysms [26, 29, 30]. It is important to note a major difference between these two model systems in that our rabbits were subjected to a purely hemodynamic insult, whereas the rodent model used hypertensive animals in which vascular inflammation could be greatly exacerbated by the actions of angiotensin II [31].

Another important difference between the current findings and previous reports is that we examined the tissue at a much earlier stage, when more immediate responses to the inciting hemodynamic insult could be assessed. We have previously documented that the WSS in the basilar artery and at the basilar terminus peaked almost immediately after the CCA ligation and then gradually reduced to the preligation baseline level within weeks [13, 32]. To our knowledge, our observations are the earliest stage at which aneurysm initiation has been examined histologically.

Our results suggest that the initial response to hemodynamic insult is destructive remodeling performed by the mural cells themselves, rather than inflammatory infiltration. Smooth muscle and endothelial cells both secrete MMPs during wound healing in vivo [18] and when directly exposed to WSS in vitro [33, 34], and we find MMP-2 and MMP-9 expressed by smooth muscle cells in response to increased flow at the basilar terminus. Thus, inflammatory infiltration is not necessary for the IEL damage and matrix degradation observed in our experiment. If it occurs, it may be a secondary event, perhaps elicited by matrix degradation products and other inflammatory signals arising from the initial response. In the rodent model systems that incorporate other manipulations, it is possible that such hemodynamically stimulated, endogenous destructive responses either precede or act in addition to the systemic, pro-inflammatory aneurysm risk factors (such as hypertension, diabetes, aging and smoking) to account for aneurysm initiation.

Our results indicate that IEL damage in response to flow insult happened while the endothelium was still present. Clearly, flow-induced aneurysm initiation does not arise simply by mechanical erosion of the wall. Rather, it is an active, cell-based remodeling process. MMP expression by mural cells may reflect a wound-like response to hemodynamic insult, with the insult being experienced initially by the endothelium. The presence of apoptotic endothelial cells in regions of IEL degradation suggests endothelial dysfunction, which could lead to MMP accumulation through (1) direct production of MMPs by the endothelial cells, (2) a leaky endothelium, exposing smooth muscle cells to blood components and activating their wound response, (3) loss of trophic signals or activation of distress signals from the endothelium to the smooth muscle, and (4) eventual loss of the endothelium, exposing smooth muscle cells directly to flow, which has been shown to induce MMP production by smooth muscle cells in vitro [35]. It is interesting to note that the expression of α-actin in smooth muscle cells was much more irregular in the basal termini that were subjected to increased flow (fig. 7). This may reflect a transition of the smooth muscle cells from their normal contractile state to the so-called 'proliferative phenotype'.

Elevation of MMP-2 and MMP-9 has been shown to occur when straight vessels undergo adaptive, expansive remodeling to accommodate a sustained increase in flow, for example after creation of an arteriovenous fistula [18] or ligation of a contralateral vessel [36]. During such adaptive expansion, the IEL is only partially degraded, developing small fenestration, presumably to permit circumferential expansion [18, 37], rather than depleted in large, continuous segments as at the basilar terminus during aneurysmal remodeling.

A notable difference between the adaptive response of a straight vessel and the response in the present, aneurysmogenic system is the pattern of MMP-2 and MMP-9 expression. During flow-induced adaptive expansion of the common carotid artery, MMP-2 expression increases at 1 or 2 days and then the high level of expression and activity is maintained until 7 days, whereas MMP-9 undergoes a transient increase in expression that peaks at 1 or 2 days then declines quickly before day 7 [18, 36]. In contrast, in our model the elevated MMP-9 levels at the basilar terminus subjected to the aneurysm-initiating hemodynamic insult were sustained for at least 5 days, while the increase in MMP-2 was transient. It is interesting to note that MMP-2 is constitutively expressed in normal healthy ar-

terial smooth muscle, whereas little or no MMP-9 is expressed in vessels that are not remodeling [38, 39]. This suggests that MMP-2 is likely to be involved in matrix turnover during routine vessel maintenance and growth, while MMP-9 expression, which correlates with IEL fenestration during expansive remodeling, may be part of a more destructive activity. MMP-9 expression may become sustained in a pathological situation, causing excessive extracellular matrix degradation and extensive IEL loss rather than transient fenestration. This may be what happens at the rabbit basilar terminus when it experiences prolonged elevated flow.

In summary, elevated flow at the rabbit basilar terminus elicits destructive remodeling responses in the arterial wall. Specifically, this condition stimulates matrix degradation, including IEL destruction, and apoptosis of endothelial, smooth muscle and adventitial cells, events that can contribute to thinning and weakening of the vessel wall and aneurysm development. These events are initiated while endothelium is present and without localized inflammatory infiltration, and thus can be attributed to local dysfunction of the endothelium and/or smooth muscle cells. Hemodynamic induction of destructive cascades in the vessel wall would help explain why intracranial aneurysms often localize to bifurcation apices and how hemodynamics can contribute to aneurysm initiation in conjunction with other risk factors.

Acknowledgments

We gratefully thank Daniel Swartz and the late Ann Marie Paciorek for assistance with surgery, Markus Tremmel and Jianping Xiang for CFD analysis, and Nicholas Liaw, Jennifer Dolan and Akira Takahashi for helpful discussions. This work was supported by the NIH (grants NS047242, NS064592) and a grant from the Interdisciplinary Research Development Fund of the University at Buffalo.

References

1 Hashimoto T, Meng H, Young WL: Intracranial aneurysms: links among inflammation, hemodynamics and vascular remodeling. Neurol Res 2006;28:372–380.
2 Stehbens WE: Etiology of intracranial berry aneurysms. J Neurosurg 1989;70:823–831.
3 Krex D, Schackert HK, Schackert G: Genesis of cerebral aneurysms – an update. Acta Neurochir (Wien) 2001;143:429–448; discussion 448–449.
4 Meng H, Wang Z, Hoi Y, Gao L, Metaxa E, Swartz DD, Kolega J: Complex hemodynamics at the apex of an arterial bifurcation induces vascular remodeling resembling cerebral aneurysm initiation. Stroke 2007;38:1924–1931.
5 Wolf RL, Imbesi SG, Galetta SL, Hurst RW, Sinson GP, Grossman RI: Development of a posterior cerebral artery aneurysm subsequent to occlusion of the contralateral internal carotid artery for giant cavernous aneurysm. Neuroradiology 2002;44:443–446.
6 Lee GY, Brophy BP: Recurrent subarachnoid haemorrhage from a de novo basilar bifurcation aneurysm: A case report. J Clin Neurosci 2003;10:250–252.
7 Hashimoto N, Handa H, Nagata I, Hazama F: Experimentally induced cerebral aneurysms in rats: Part v. Relation of hemodynamics in the circle of willis to formation of aneurysms. Surg Neurol 1980;13:41–45.
8 Aoki T, Nishimura M: Targeting chronic inflammation in cerebral aneurysms: Focusing on NF-κB as a putative target of medical therapy. Expert Opin Ther Targets;14:265–273.
9 Eldawoody H, Shimizu H, Kimura N, Saito A, Nakayama T, Takahashi A, Tominaga T: Fasudil, a rho-kinase inhibitor, attenuates induction and progression of cerebral aneurysms: experimental study in rats using vascular corrosion casts. Neurosci Lett 2010;470:76–80.
10 Tada Y, Kitazato KT, Tamura T, Yagi K, Shimada K, Kinouchi T, Satomi J, Nagahiro S: Role of mineralocorticoid receptor on experimental cerebral aneurysms in rats. Hypertension 2009;54:552–557.
11 Hassler O: Experimental carotid ligation followed by aneurysmal formation and other morphological changes in the circle of willis. J Neurosurg 1963;20:1–7.
12 Metaxa E, Tremmel M, Natarajan SK, Xiang J, Paluch RA, Mandelbaum M, Siddiqui AH, Kolega J, Mocco J, Meng H: Characterization of critical hemodynamics contributing to aneurysmal remodeling at the basilar terminus in a rabbit model. Stroke 2010;41:1774–1782.
13 Meng H, Metaxa E, Gao L, Liaw N, Sabareesh K, Swartz D, Siddiqui A, Kolega J, Mocco J: Progressive aneurysm development following hemodynamic insult. J Neurosurg 2011;114:1095–1103.
14 Kamiya A, Togawa T: Adaptive regulation of wall shear stress to flow change in the canine carotid artery. Am J Physiol 1980;239:H14–21.
15 Kamiya A, Bukhari R, Togawa T: Adaptive regulation of wall shear stress optimizing vascular tree function. Bull Math Biol 1984;46:127–137.
16 Gibbons GH, Dzau VJ: The emerging concept of vascular remodeling. N Engl J Med 1994;330:1431–1438.
17 Sho E, Komatsu M, Sho M, Nanjo H, Singh TM, Xu C, Masuda H, Zarins CK: High flow drives vascular endothelial cell proliferation during flow-induced arterial remodeling associated with the expression of vascular endothelial growth factor. Exp Mol Pathol 2003;75:1–11.
18 Sho E, Sho M, Singh TM, Nanjo H, Komatsu M, Xu C, Masuda H, Zarins CK: Arterial enlargement in response to high flow requires early expression of matrix metalloproteinases to degrade extracellular matrix. Exp Mol Pathol 2002;73:142–153.
19 Kataoka K, Taneda M, Asai T, Kinoshita A, Ito M, Kuroda R: Structural fragility and inflammatory response of ruptured cerebral aneurysms. A comparative study between ruptured and unruptured cerebral aneurysms. Stroke 1999;30:1396–1401.
20 Frosen J, Piippo A, Paetau A, Kangasniemi M, Niemela M, Hernesniemi J, Jaaskelainen J: Remodeling of saccular cerebral artery aneurysm wall is associated with rupture: histological analysis of 24 unruptured and 42 ruptured cases. Stroke 2004;35:2287–2293.
21 Gao L, Hoi Y, Swartz DD, Kolega J, Siddiqui A, Meng H: Nascent aneurysm formation at the basilar terminus induced by hemodynamics. Stroke 2008;39:2085–2090.

22 Meng H, Swartz DD, Wang Z, Hoi Y, Kolega J, Metaxa EM, Szymanski MP, Yamamoto J, Sauvageau E, Levy EI: A model system for mapping vascular responses to complex hemodynamics at arterial bifurcations in vivo. Neurosurgery 2006;59:1094–1100; discussion 1100–1001.
23 Tremmel M, Xiang J, Hoi Y, Kolega J, Siddiqui AH, Mocco J, Meng H: Mapping vascular response to in vivo hemodynamics: application to increased flow at the basilar terminus. Biomech Model Mechanobiol 2010;9:421–434.
24 Pham NA, Morrison A, Schwock J, Aviel-Ronen S, Iakovlev V, Tsao MS, Ho J, Hedley DW: Quantitative image analysis of immunohistochemical stains using a cmyk color model. Diagn Pathol 2007;2:8.
25 Stehbens WE: Pathology of the Cerebral Blood Vessels. Saint Louis, C. V. Mosby, 1972.
26 Aoki T, Kataoka H, Morimoto M, Nozaki K, Hashimoto N: Macrophage-derived matrix metalloproteinase-2 and -9 promote the progression of cerebral aneurysms in rats. Stroke 2007;38:162–169.
27 Bruno G, Todor R, Lewis I, Chyatte D: Vascular extracellular matrix remodeling in cerebral aneurysms. J Neurosurg 1998;89:431–440.
28 Kim SC, Singh M, Huang J, Prestigiacomo CJ, Winfree CJ, Solomon RA, Connolly ES Jr: Matrix metalloproteinase-9 in cerebral aneurysms. Neurosurgery 1997;41:642–666; discussion 646–647.
29 Aoki T, Kataoka H, Ishibashi R, Nozaki K, Egashira K, Hashimoto N: Impact of monocyte chemoattractant protein-1 deficiency on cerebral aneurysm formation. Stroke 2009;40:942–951.
30 Aoki T, Kataoka H, Ishibashi R, Nozaki K, Hashimoto N: Simvastatin suppresses the progression of experimentally induced cerebral aneurysms in rats. Stroke 2008;39:1276–1285.
31 Ruiz-Ortega M, Esteban V, Ruperez M, Sanchez-Lopez E, Rodriguez-Vita J, Carvajal G, Egido J: Renal and vascular hypertension-induced inflammation: Role of angiotensin ii. Curr Opin Nephrol Hypertens 2006;15:159–166.
32 Hoi YGL, Tremmel M, Paluch RA, Siddiqui AH, Meng H, Mocco J: In vivo assessment of rapid cerebrovascular morphologic adaptation following acute blood flow increase. J Neurosurg 2008;109:1141–1149.
33 Magid R, Murphy TJ, Galis ZS: Expression of matrix metalloproteinase-9 in endothelial cells is differentially regulated by shear stress. Role of c-myc. J Biol Chem 2003;278:32994–32999.
34 Sakamoto N, Ohashi T, Sato M: Effect of fluid shear stress on migration of vascular smooth muscle cells in cocultured model. Ann Biomed Eng 2006;34:408–415.
35 Cullen JP, Sayeed S, Kim Y, Theodorakis NG, Sitzmann JV, Cahill PA, Redmond EM: Ethanol inhibits pulse pressure-induced vascular smooth muscle cell migration by differentially modulating plasminogen activator inhibitor type 1, matrix metalloproteinase-2 and -9. Thromb Haemost 2005;94:639–645.
36 Nuki Y, Matsumoto MM, Tsang E, Young WL, van Rooijen N, Kurihara C, Hashimoto T: Roles of macrophages in flow-induced outward vascular remodeling. J Cereb Blood Flow Metab 2009;29:495–503.
37 Tronc F, Mallat Z, Lehoux S, Wassef M, Esposito B, Tedgui A: Role of matrix metalloproteinases in blood flow-induced arterial enlargement: Interaction with no. Arterioscler Thromb Vasc Biol 2000;20:E120–126.
38 Galis ZS, Muszynski M, Sukhova GK, Simon-Morrissey E, Unemori EN, Lark MW, Amento E, Libby P: Cytokine-stimulated human vascular smooth muscle cells synthesize a complement of enzymes required for extracellular matrix digestion. Circ Res 1994;75:181–189.
39 Galis ZS, Sukhova GK, Lark MW, Libby P: Increased expression of matrix metalloproteinases and matrix degrading activity in vulnerable regions of human atherosclerotic plaques. J Clin Invest 1994;94:2493–2503.